Available online at www.sciencedirect.com
SCIENCE DIRECT
Journal of Molecular Structure 795 (2006) 198–208
Journal of MOLECULAR STRUCTURE
www.elsevier.com/locate/molstruc

Millimeter-wave study of the CO–N_2 van der Waals complex: new measurements of CO–*ortho*N_2 and assignments of new states of CO–*para*N_2

L.A. Surin [a,b,*], A.V. Potapov [b], H.S.P. Müller [a], V.A. Panfilov [b], B.S. Dumesh [b], T.F. Giesen [a], S. Schlemmer [a]

[a] *I.Physikalisches Institut, Universität zu Köln, Zülpicher Str. 77, 50937 Cologne, Germany*
[b] *Institute of Spectroscopy, Russian Academy of Sciences, 142190 Troitsk, Moscow, Russian*

Received 19 December 2005; received in revised form 1 February 2006; accepted 16 February 2006
Available online 18 April 2006

Abstract

Rotational transitions of the CO–N_2 van der Waals complex have been measured using the intracavity OROTRON jet spectrometer in the frequency range of 83–133 GHz. For the CO–*ortho*N_2 spin modification, the observed and assigned 21 rotational transitions belong to the *Q*- and *P*-branches of the $K=1$–0 subband. They complete the previous observation of the corresponding *R*-branch transitions. In the case of the less abundant form, CO–*para*N_2, a new $K=1$ state, representing simultaneous rotation of both monomers, was detected for the first time. A total of 31 rotational transitions of CO–*para*N_2 were assigned to two subbands connecting this new $K=1$ state with already known lower $K=0$ and 1 states. The assignments relied in part on energy level differences obtained from precise microwave data. The origin of the newly observed state was determined to be 3.41 cm^{-1} relative to the $K=0$ ground state of CO–*para*N_2. The analysis yielded rotational parameters, centrifugal distortion parameters and nuclear quadrupole coupling constants due to the presence of two equivalent ^{14}N nuclei for both CO–*ortho*N_2 and CO–*para*N_2.

Keywords: Millimeter-wave spectroscopy; van der Waals complex; CO–N_2 complex; Internal rotation; Quadrupole coupling; OROTRON

1. Introduction

Complexes containing CO molecules and light rare gas atoms (Rg = He, Ne, Ar) or nonpolar molecules (N_2, H_2, D_2) have extremely low binding energies and show various types of intermolecular motions. The first group of such species, Rg–CO, has been well studied over the last years in the infrared (IR), microwave (MW) and millimeter-wave ranges demonstrating the hindered internal rotation of the CO subunit and the transformation of spectra from the semi-rigid rotor approximation in the case of Ar–CO [1] and Ne–CO [2] to the free rotor basis in case of He–CO [3,4]. Complexes containing the CO molecule and nonpolar diatomics like N_2, H_2 or D_2 exhibit evidently more complicated spectra. But if the diatomics N_2 or H_2, D_2 are in the pure rotationless $j=0$ states, they can be related also to Rg–CO complexes in some respect. The corresponding spectra of CO–*para*H_2 ($j_{H_2}=0$) and CO–*ortho*D_2 ($j_{D_2}=0$) have been studied already in the IR and millimeter-wave regions [5–8]. The spectrum of CO–*ortho*H_2 ($j_{H_2}=1$) has been recorded by McKellar in IR [5] as well as in the course of our separate survey in the millimeter-wave range but is not yet understood or analyzed.

For the CO–N_2 complex, the rotationless $j_{N_2}=0$ states are associated with the *ortho*N_2 spin modification with total nuclear spin quantum number $I=0$ and 2. The states involving $j_{N_2}=1$ internal rotational excitation are associated with *para*N_2 with $I=1$. The latter modification, related to CO–*ortho*H_2, displays a more complicated spectral pattern and gives valuable information on the dependence of the potential not only on the CO but also on the N_2 orientation in the complex.

Theoretical work on the CO–N_2 intermolecular potential comprises only the semiempirical result reported by Francken and Dykstra [9] and an ab initio study by Fišer et al. [10,11]. The experimental studies are more extensive. First works on CO–N_2 were made in the 4.7 μm infrared (IR) region of the CO stretching vibration by Kawashima and Nishizawa [12] using a pulsed molecular beam and by Xu and McKellar [13] using a continuous slit-jet nozzle expansion, both combined with a diode laser spectrometer.

* Corresponding author. Address: I.Physikalisches Institut, Universität zu Köln, Zülpicher Str. 77, 50937 Cologne, Germany. Tel.: +49 221 4703560; fax: +49 221 4705162.
E-mail address: surin@phl.uni-koeln.de (L.A. Surin).

0022-2860/$ - see front matter © 2006 Elsevier B.V. All rights reserved.
doi:10.1016/j.molstruc.2006.02.027

The latter authors [13] performed a more detailed analysis, assigning four connected subbands to the $K=0$, 1, and 2 states, as well as one separate subband to a $K=1$ state. The four connected subbands were attributed to transitions involving the rotationless $j_{N_2}=0$ states and the separate subband was tentatively assigned to transitions involving $j_{N_2}=1$ states. Using the prediction from these IR works [12,13], the microwave observations [14–16] of $K=0$, 1 states for both spin modifications as well as millimeter wave study [15] of $K=1$–0 R-branch transitions for CO–*ortho*N_2 have been made. In more recent work of Xia et al. [17], the IR spectrum of the CO–N_2 complex has been studied in further detail, extending the previous tentative assignment of just one subband in CO–*para*N_2 to include more than 10 linked subbands. In the same work, two new subbands in CO–*ortho*N_2 were observed, which involved an excited bending state with an energy of about 4.7 cm^{-1}. The direct observation of this bending vibration using the OROTRON spectrometer was reported subsequently [18].

In this paper, we present new survey spectroscopic investigations of CO–N_2 with the OROTRON spectrometer in the frequency range of 83–133 GHz. It resulted, first, in the observation of the Q- and P-branches of the $K=1$–0 subband of the CO–*ortho*N_2 spin modification, thus completing our previous observation of the R-branch transitions [15] and giving information on asymmetry splitting in the $K=1$ state. Second, two connected subbands, $K=1$–0 and $K=1$–1, were observed and assigned for the less abundant form, CO–*para*N_2. The new upper state with $K=1$ located at 3.41 cm^{-1} relative to the lowest $K=0$ state of CO–*para*N_2 was observed for the first time. This state represents simultaneous nearly free rotation of both monomers. Nuclear quadrupole splitting due to two equivalent ^{14}N nuclei was resolved to a varying degree for both spin modifications yielding additional information about the angular orientation and dynamics of the N_2 subunit within the complex.

2. Experimental

The millimeter wave spectra of CO–N_2 (both *ortho*N_2 and *para*N_2) have been measured in the frequency range of 83–133 GHz using the intracavity jet spectrometer, OROTRON. Details of the set-up were given elsewhere [19]. Briefly, the home-made millimeter-wave generator OROTRON is placed in the vacuum chamber together with the supersonic jet apparatus. The molecular beam is injected into the OROTRON cavity perpendicularly to its axis. The high Q-factor of the cavity results in 100 effective passes of the radiation through the jet. Absorption in the cavity causes changes of the electron current in the collector circuit of the OROTRON and is detected very sensitively by measuring these current changes. A small part of the millimeter-wave radiation is coupled out of cavity through openings in the spherical mirror and mixed with the radiation of an HP 8671B microwave synthesizer for frequency determinations.

The experiment was performed with a pin-hole pulsed jet source, General Valve, Series 9. The diameter of the nozzle was 0.8 mm, and the typical repetition rate was 10 Hz. The pumping system utilized an Edwards 9B3K Booster pump and as backing a Pfeiffer DUO 20 M rotary pump. We used a gas mixture of 1% of CO and 1% of N_2 in Ne at a backing pressure of 3.5 bar. The frequency of the OROTRON was modulated at 25 kHz by a sinewave. The collector signal was demodulated by a digital lock-in amplifier operated in $2f$ mode with a time constant of 160 μs. The output of the lock-in was then processed by a gated integrator with a time constant of 1 s. For most of the absorption measurements, the full linewidth at half height (FWHH) is about 300 kHz and the accuracy of line center positions is estimated to be about 50 kHz.

Transitions of the Ne–CO complex and the CO-dimer were also observed in the spectrum but they could be easily distinguished from CO–N_2 lines due to our previous millimeter-wave survey of both, Ne–CO [2] and $(CO)_2$ [20,21]. The hyperfine structure due to two ^{14}N quadrupole nuclei was very useful for assigning spectral features to CO–N_2.

3. Energy levels for the CO–N_2 complex

As was shown in previous studies [12–18], it is useful to consider the CO–N_2 complex in terms of almost free internal rotation. The energy levels of the complex in the free rotation limit will be the sum of the individual CO and N_2 monomer rotational energies and the end-over-end rotational energy of the complex. The corresponding sums of monomer rotational energies for the range 0–20 cm^{-1} are shown in the middle diagram of Fig. 1 as given by Xu and McKellar [13]. The energy levels are labeled by j_{CO} and j_{N_2}, referring to the rotation of the CO and N_2 subunits, and they are divided into two distinct groups, corresponding to complexes involving *ortho*N_2 or *para*N_2 spin modifications. Transitions between these two modifications are forbidden in general, and the allowed transitions involve a change of one in CO rotation state, $\Delta j_{CO}=\pm 1$, and no change in the N_2 state, $\Delta j_{N_2}=0$, as indicated by the vertical lines.

Each (j_{CO}, j_{N_2}) state forms the foundation for a number of stacks of end-over-end rotational levels. In the free rotation limit, the stacks from a given (j_{CO}, j_{N_2}) state are degenerate, but due to the influence of the intermolecular forces they separate. The corresponding stack origins are shown for CO–*ortho*N_2 and CO–*para*N_2 in the left and right diagrams of Fig. 1, respectively. The stacks are distinguished by different values of $K=K_a$, the projection of angular momentum J on the intermolecular axis a. For example, the $(j_{CO}, j_{N_2})=(0,0)$ state has a single stack with $K=0$ representing the ground state of CO–*ortho*N_2 (left diagram of Fig. 1). The $(j_{CO}, j_{N_2})=(1,0)$ state forms a pair of stacks with $K=1$ corresponding to rotation of the CO unit around the intermolecular a-axis and one stack with $K=0$, which has the nature of a CO bending vibration. The splitting of the $K=1$ stack into two is due to asymmetry of the complex (different B and C rotational constants). The labels e and f determine the parity of J levels within a given stack. The parity of an even-J level is + for stacks

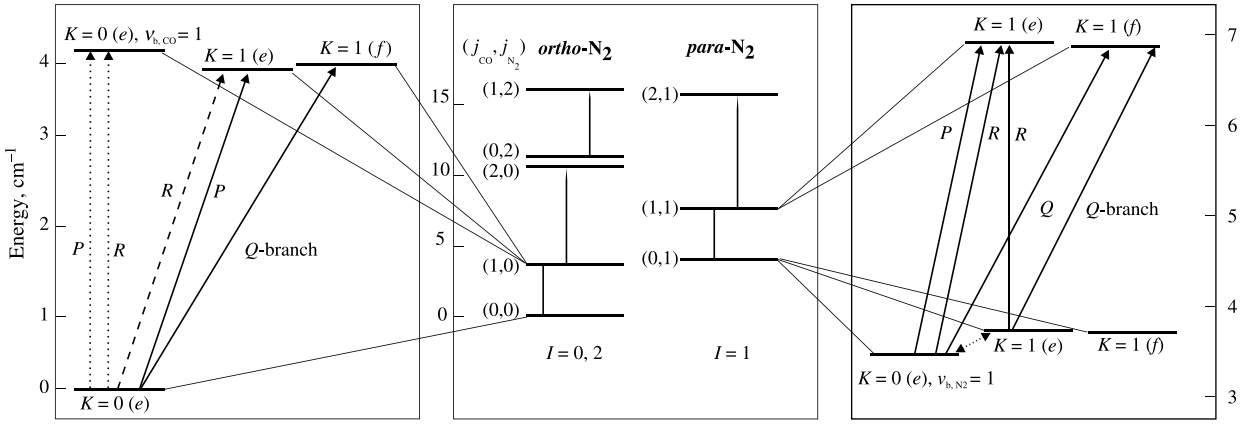

Fig. 1. Rotational energy state origins for the CO–N_2 complex in the limit of free internal rotation of the CO and N_2 (middle diagram as given in Ref. [13]). The states are divided into two spin modifications: *ortho*N_2 with total nuclear spin $I=0$ and 2, and *para*N_2 with total nuclear spin $I=1$. The allowed transitions are indicated by vertical lines. The influence of the intermolecular forces splits free rotor states as shown in the left and right diagrams for CO–*ortho*N_2 and CO–*para*N_2, respectively. Some of the states take the character of CO or N_2 bending vibrations. Only stack origins of end-over-end rotational levels are depicted. The stacks are distinguished by different values of K, the projection of the angular momentum J on the intermolecular axis. The labels e and f determine the parity of J levels within a given stack. Previously observed subbands [15,16,18] connecting different stacks of levels are marked by dashed and dotted arrows. The a-type $\Delta K=0$ transitions within the $K=0$ and $K=1(e)$ stacks of CO–*ortho*N_2 and within low $K=0$, $K=1(e)$ and $K=1(f)$ stacks of CO–*para*N_2 were also detected [14,15,16] but not shown in the diagrams. The new subbands measured in the present work are indicated by solid arrows.

labeled by e and $-$ for f, while the parity of an odd-J level is $-$ for e and $+$ for stacks labeled by f.

The previously measured subbands of CO–*ortho*N_2 [15,18] are shown by dashed and dotted lines on the left diagram of Fig. 1. The microwave a-type transitions within $K=0$ ground state and within $K=1(e)$ state, not depicted here, were also measured [14,15]. The Q- and P-branches of the $K=1$–0 subband observed in the present study are shown by solid lines.

The lowest state of the CO–*para*N_2, $(j_{CO}, j_{N_2})=(0,1)$, consists of the three closely spaced stacks as shown in the right diagram of Fig. 1. This state was well characterized recently in a MW study by Xu and Jäger [16]. They observed and analyzed the a-type rotational transitions within the relatively unperturbed $K=1(f)$ levels (these transitions are not shown in the diagram) previously studied in the infrared region by Xu and McKellar [13]. In addition, they investigated two new states, namely the $K=0$ levels of the first excited van der Waals N_2 bending state and the $K=1(e)$ levels of the ground vibrational state of CO–*para*N_2. Both a-type rotational transitions within these two stacks (not shown in the diagram) and b-type ro-vibrational transitions connecting these two stacks (dotted line in right diagram of Fig. 1) were detected. It was shown that a strong Coriolis interaction occurs between these two states.

The higher state of CO–*para*N_2 with excited rotation of the CO unit, i.e. $(j_{CO}, j_{N_2})=(1,1)$, is more complicated. This state includes nine stacks with $K=0$, 1, 2, which are located 3–5 cm^{-1} above the ground state of CO–*para*N_2 [17]. Two of them were detected for the first time in the present work and the corresponding observed branches of transitions are shown in the right diagram of Fig. 1 by solid lines. A schematic energy level diagram of CO–*para*N_2 as determined in present work and in previous MW study [16] is shown in Fig. 2.

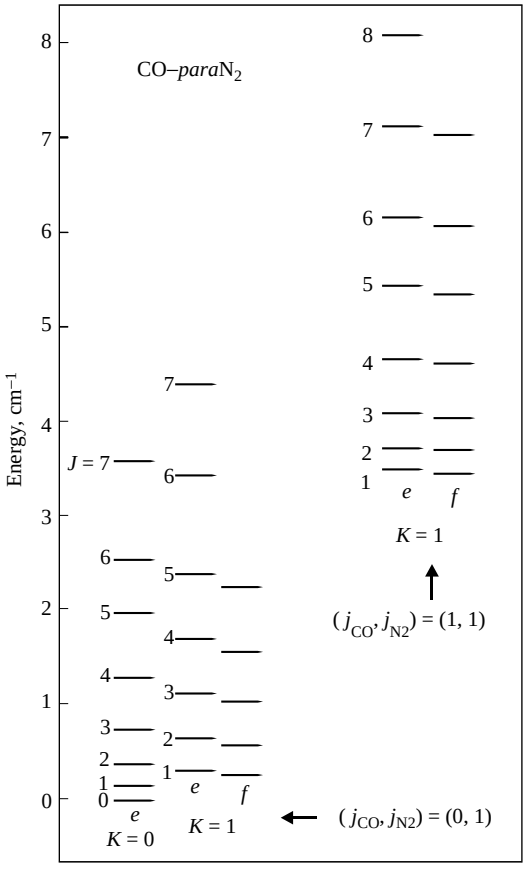

Fig. 2. Schematic energy level diagram of CO–*para*N_2 for the lowest state $(j_{CO}, j_{N_2})=(0,1)$ and for the upper state $(j_{CO}, j_{N_2})=(1,1)$ as determined in the present work. The lowest $J=K=0$ level is set to zero energy. The upper $K=1$ levels belong to two of nine stacks of levels expected for the $(j_{CO}, j_{N_2})=(1,1)$ free rotor state of CO–*para*N_2, where j_{CO} and j_{N_2} refer to the rotational angular momenta of CO and N_2, respectively. The parity of an even-J level is $+$ for stacks labeled by e and $-$ for f, while the parity of an odd-J level is $-$ for e and $+$ for stacks labeled by f.

4. Results and analysis

4.1. CO–orthoN$_2$

Twenty-one rotational transitions in the frequency range from 84 to 104 GHz were measured and assigned on the basis of molecular constants from the IR work of Xu and McKellar [13]. These are three *P*-branch and 18 *Q*-branch perpendicular transitions from the $K=0$ ground state to the $K=1$ state of CO–*ortho*N_2. The maximum *J*-value is 18 as compared to 17 in the IR experiments [12,13]. The differences between the observed frequencies and those predicted from IR data were less than 10 MHz for the low *J*-values. To predict accurately higher-*J* transitions, the already determined frequencies of the preceding transitions were taken into account. The new measurements complete our previous observation of the *R*-branch transitions of CO–*ortho*N_2 of the same $K=1$–0 subband [15]. The newly (solid line) and previously (dashed and dotted lines) observed subbands are shown in the left diagram of Fig. 1. The assignments of *P*(2), *P*(3) and *P*(4) transitions were further confirmed through the combination differences from the precise MW and millimeter-wave data [15]. Most of the observed lines display ^{14}N hyperfine structure. As an example, the *Q*(10) transition is shown in Fig. 3 together with a simulation of the spectrum obtained from the final set of spectroscopic parameters. The measured transitions frequencies, assignments, uncertainties and residuals are listed in Table 1.

The newly determined line frequencies together with available MW and millimeter-wave data on CO–*ortho*N_2 [15,18] were used to fit simultaneously the band origin σ, the rotational and centrifugal distortion parameters along with the nuclear quadrupole coupling constants χ_{aa}, χ_{bb} for $K=0$ and 1 employing an exact diagonalization program [22]. The $K=1(e)$ and $K=1(f)$ states were fitted as two asymmetry components of one $K=1$ state. The rotational and centrifugal distortion terms were expanded in $J(J-1)-K^2$ as in previous works [13,15].

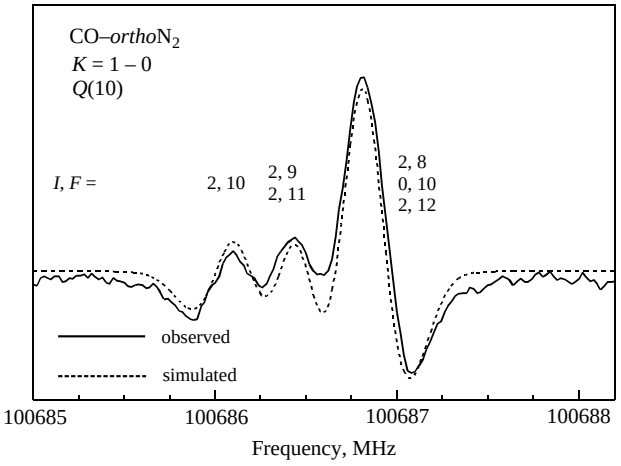

Fig. 3. Recording of the $K=1$–0 *Q*(10) rotational transition of the CO–*ortho*N_2 spin modification together with a simulation of the spectrum obtained from the final set of spectroscopic parameters. The nuclear quadrupole structure due to two equivalent ^{14}N nuclei is partly resolved.

Fitting both $K=1(e)$ and $K=1(f)$ with separate *B*, *D*, etc. values resulted in considerably larger residuals. However, it was found that the higher *J*-transitions required slightly different values for χ_{bb} and a centrifugal distortion correction χ_{aa_J} for $K=1(f)$. This parameter was also included for the $K=0$ state. The χ_{aa_J} values for $K=0$ and $K=1(f)$ are very similar. Thus, the slightly different values of χ_{bb} for $K=1(e)$ and $1(f)$ and the fact that it was more useful constraining χ_{aa_J} of $K=1(e)$ to 0 rather than to the value of $K=1(f)$ may indicate a weak perturbation of $K=1(e)$.

Each line consisting of overlapping hyperfine components was treated as the intensity weighted average of the individual components. Contributions of components weaker than the strongest one by more than a factor of 10 were not considered. Because of the overlap and the proximity of the hyperfine components, simulations were made to determine the differences between the intensity weighted average line positions and the apparent peak positions. Second derivatives line shapes were calculated in which each hyperfine component was represented by a Gaussian line profile of 300 kHz FWHH. The corrections applied were mostly below the 50 kHz uncertainties of the lines.

The resulting spectroscopic parameters are given in Table 2 together with previous values from an infrared study [13]. The present and the previous values for the band origin σ and the rotational constant *B* are in good agreement. The values for *D* are similar. The standard deviations of the fit was 39 and 16 kHz for the newly recorded $K=1$–0 *Q*- and *P*-branch transitions, respectively. The previously recorded [15] $\Delta K=0$ transitions within $K=0$ and 1 states were reproduced within 3.0 kHz, while the $K=1$–0 *R*-branch transitions were reproduced within 63 kHz.

4.2. CO–paraN$_2$

In the case of the CO–*para*N_2 spin modification, we searched for the transitions between $(j_{CO}, j_{N_2})=(1,1)$ and (0,1) states (see Fig. 1). They were expected to be at frequencies of 3–5 cm^{-1}. Ultimately, the frequency range covered was 83–133 GHz including some selected measurements up to 160 GHz. Compared to the total number of observed transitions (about 100), only 31 transitions could be assigned at present. The starting point for the assignment process of the observed transitions rests on the MW study by Xu and Jäger [16]. They determined accurately the energy levels up to $J=6$ of the lower $(j_{CO}, j_{N_2})=(0,1)$ state (see Fig. 2). We calculated all possible differences between the measured frequencies and compared them with the differences between the energies of appropriate energy levels within the $(j_{CO}, j_{N_2})=(0,1)$ state. A number of reasonable combination differences was found for the low-*J* levels belonging to the $K=0$ and $K=1(e)$ stacks of the $(j_{CO}, j_{N_2})=(0,1)$ state. The appropriate coincidence in frequency and energy differences was better than 500 kHz, i.e. within a typical hyperfine splitting pattern limiting the application of a more precise criterion. The identified transitions connected these lower stacks with the newly observed pair of $K=1$ stacks of the $(j_{CO}, j_{N_2})=(1,1)$

Table 1
Assigned $K=10$ rotational transitions of the CO–*ortho*N_2 complex, their frequencies[a] and residuals

J'–J''	I', F'–I'', F''	Frequency (MHz)	Observed − calculated (kHz)
1–2	2,3–2,4	94591.794	−7
2–3	2,2–2,3;2,3–2,4	89550.730	−34
	2,4–2,5;2,1–2,2;0,2–0,3	89551.398	−14
3–4	2,3–2,4	84216.559	2
	2,4–2,5	84216.867	−2
	2,2–2,3;2,5–2,6;0,3–0,4;2,1–2,2	84217.506	−10
1–1	2,1–2,2;2,1–0,1	103749.560	0[b]
	2,3–2,2;2,3–2,3	103750.102	1
	0,1–2,2;0,1–0,1;2,2–2,2;2,2–0,1;2,2–2,3;0,1–2,1;2,2–2,1	103750.500	24[c]
2–2	2,4–2,4	103660.278	−33
3–3	2,3–2,3;2,4–2,4	103521.665	49
	2,2–2,2;2,5–2,5;0,3–0,3	103521.961	8
4–4	2,4–2,4;2,5–2,5	103330.533	75
	2,6–2,6;0,4–0,4;2,2–2,2	103330.898	16
5–5	2,5–2,5	103080.995	66
	2,4–2,4;2,7–2,7;0,5–0,5;2,3–2,3	103081.510	47
6–6	2,6–2,6	102766.380	5
	2,7–2,7	102766.590	−20
	2,8–2,8;0,6–0,6;2,4–2,4	102766.938	−33
7–7	2,7–2,7	102378.635	−46
	2,8–2,8;2,6–2,6	102378.920	−65
	2,9–2,9;0,7–0,7;2,5–2,5	102379.262	−33
8–8	2,8–2,8	101908.925	−23
	2,9–2,9;2,7–2,7	101909.214	−43
	2,10–2,10;0,8–0,8;2,6–2,6	101909.542	−29
9–9	2,9–2,9	101347.806	−6
	2,10–2,10;2,8–2,8	101348.127	1
	2–11–2,11;0,9–0,9;2,7–2,7	101348.449	6
10–10	2,10–2,10	100686.122	19
	2,11–2,11;2,9–2,9	100686.448	28
	2,12–2,12;0,10–0,10;2,8–2,8	100686.792	53
11–11	2,11–2,11	99915.871	35
	2,12–2,12;2,10–2,10	99916.189	34
	2,13–2,13;0,11–0,11;2,9–2,9	99916.536	60
12–12	2,12–2,12	99031.702	−5
	2,13–2,13;2,11–2,11	99032.033	5
	2,14–2,14;0,12–0,12;2,10–2,10	99032.373	23
13–13	2,13–2,13	98033.227	−56
	2,14–2,14;2,12–2,12	98033.577	−28
	2,15–2,15;0,13–0,13;2,11–2,11	98033.890	−38
14–14	2,14–2,14	96928.113	−60
	2,15–2,15;2,13–2,13	96928.461	−35
	2,16–2,16;0,14–0,14;2,12–2,12	96928.764	−55
15–15	2,15–2,15	95736.529	54
	2,16–2,16;2,14–2,14	95736.873	75
	2,17–2,17;0,15–0,15;2,13–2,13	95737.148	26
16–16	2,17–2,17;2,15–2,15	94497.020	15
	2,18–2,18;0,16–0,16;2,14–2,14	94497.370	41
17–17	2,19–2,19;0,17–0,17;2,15–2,15	93273.275	−85
18–18	2,20–2,20;0,18–0,18;2,16–2,16	92160.980	21

[a] Experimental uncertainties estimated to be 50 kHz.
[b] Fit as difference between this and central component: 542 ± 20 kHz, observed − calculated = 0 kHz.
[c] Fit as difference between this and central component: 398 ± 30 kHz, observed − calculated = 24 kHz.

state. Several transitions involving higher-J values as available from MW study [16] were predicted and assigned in the process of fitting and analyzing the data. The $K=1(e)$–0 $R(1)$ line is presented in Fig. 4 and demonstrates a rather extensive hyperfine structure and the ability of our spectrometer to resolve this pattern. In total, five branches of two $K=1$–0 and $K=1$–1 subbands were observed as shown in Fig. 1 in the right diagram. A schematic energy level diagram of CO–*para*N_2 as determined in the present work and in the previous MW study [16] is shown in Fig. 2. The measured frequencies of identified transitions, their assignments, uncertainties and residuals are listed in Table 3. Most of the lines display ^{14}N hyperfine

Table 2
Spectroscopic parameters (in MHz) of the $K=0$ and 1 states of CO–*ortho*N_2

	$K=0$		$K=1$	
	Present	Previous	Present	Previous
σ			105936.70748(281)	105935.86(60)[a]
B	2227.54180(39)	2227.392(66)[a]	2141.98210(96)	2141.990(87)[a]
D	0.133161(57)	0.1296(15)[a]	0.202711(50)	0.2073(16)[a]
$H\times10^3$	−0.05587(298)	−0.079(10)[a]	−0.00839(185)	0.0075(89)[a]
$L\times10^6$	−0.039(43)	−0.10(23)[a]	0.4688(243)	
$M\times10^9$	−4.74(38)		−4.32(38)	
$N\times10^{12}$	−6.59(93)		−5.32(81)	
B			126.20000(212)	126.009(120)[a]
D			0.031320(104)	0.0407(16)[a]
$H\times10^3$			−0.08906(318)	−0.002159(45)[a]
$L\times10^6$			−0.722(53)	
$M\times10^9$			−1.092	
$N\times10^{12}$			−1.916(246)	
χ_{aa}	0.20503(147)	0.19641(52)[b]	−1.03933(165)	−1.0391(17)[b]
$\chi_{aa\_j}\times10^3$	−2.175(246)		—/−2.10(35)[c]	
χ_{bb}			0.06064(170)/0.1660(266)[c]	0.0633(17)[b]

[a] Values from work of Xia et al. [17] converted from cm^{-1} to MHz units.
[b] Values from work of Xu et al. [15].
[c] The first value is given for $K=1(e)$ state, the second value is given for $K=1(f)$ state.

structure and the frequencies of all resolved peaks are given with corresponding hyperfine labels I, F.

The newly determined line frequencies together with available MW data on CO–*para*N_2 [16] were used to fit simultaneously the band origins σ, the rotational and centrifugal distortion parameters and the nuclear quadrupole coupling constants χ_{aa}, χ_{bb} for $K=0$ and 1 for both $(j_{CO}, j_{N_2})=(0,1)$ and (1,1) states employing an exact diagonalization program [22], similar to CO–*ortho*N_2 spin modification. The $K=1(e)$ and $K=1(f)$ doublet of the $(j_{CO}, j_{N_2})=(1,1)$ state was fitted as two asymmetry components of one $K=1$ state. In contrast, both components, $K=1(e)$ and $K=1(f)$, of the $(j_{CO}, j_{N_2})=(0,1)$ state were fitted with separate B, D, etc. following Xu and Jäger [16]. It was also found that inclusion of the centrifugal distortion correction χ_{aa_J} or χ_{bb_J}, as well as the spin-rotation constant for $K=0$ and 1 of the $(j_{CO}, j_{N_2})=(0,1)$ state improved the quality of the fit substantially.

The hyperfine structure of the new $K=1$ levels was fairly straightforward to analyze. The analysis started with low-J transitions of the $K=1(e)$–0 R-branch and of the $K=1(f)$–0 Q-branch. Both $J=1$–0 and $J=2$–2 transitions suggested $\chi_{bb}\approx0$. Simulation of the $J=4$ and 5 Q-branch transitions yielded good estimates for χ_{aa} whose value was secured with the assignment of the $R(1)$ transition shown in Fig. 4. The slightly broader $F=1$–0 component causes it to appear seemingly weaker than the $F=2$–2 component, in contrast to the simulation with equal line widths for all components. The spectroscopic parameters obtained for the new and previously observed states are given in Table 4.

The parameters of the CO–*para*N_2 levels already analyzed by Xu and Jäger [16] are in good agreement with their values for the $K=1(f)$ state while those for Coriolis coupled $K=0$ and $K=1(e)$ states show somewhat larger deviations which are caused by a slightly different hyperfine analysis, by the inclusion of G_{JJ} in our fit and by the additional information originating from our new data. These transitions have been reproduced to within 3.0 kHz. The generally larger uncertainties in the present work are caused by larger assumed experimental uncertainties of 5 kHz for the FTMW transitions here while Xu and Jäger [16] probably used 1 kHz. The new lines were reproduced within 25 kHz.

It can be seen from Table 4 that the previously observed $K=1$ stacks of the $(j_{CO}, j_{N_2})=(0,1)$ state have very different χ_{bb} values even though they appear to be the two asymmetry components of one $K=1$ state, while the new $K=1$ levels of the (1,1) state were described by just one χ_{aa} and one χ_{bb}. As mentioned, this series of

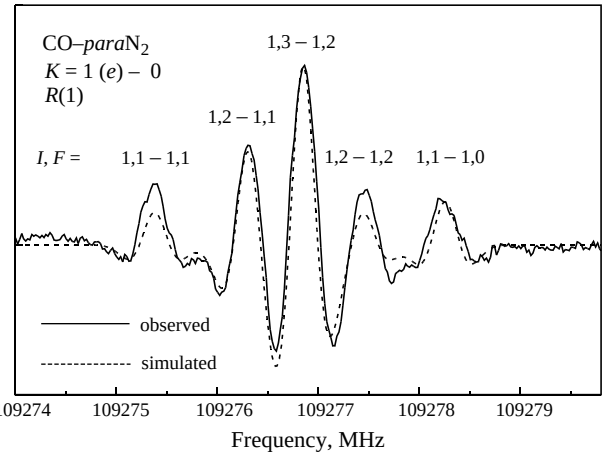

Fig. 4. Recording of the $(j_{CO}, j_{N_2})=(1,1)-(0,1)$, $K=1(e)$–0 $R(1)$ rotational transition of the CO–*para*N_2 spin modification together with a simulation of the spectrum obtained from the final set of spectroscopic parameters. The nuclear quadrupole structure due to two equivalent ^{14}N nuclei is completely resolved.

Table 3
Assigned $K=1$–0 and $K=1$–1 rotational transitions of CO–*para*N_2, their frequencies[a] and residuals

J'–J''	I', F'–I'', F''	Frequency (MHz)	Observed − calculated (kHz)
$K=1(e)$–0			
1–2	1,1–1,2;1,2–1,2	94205.171	−9
	1,2–1,3	94206.170	−4
	1,0–1,1	94205.747	−2
2–3	1,2–1,3	90913.064	1
	1,3–1,4;1,1–1,2	90913.380	−16
3–4	1,3–1,4;1,2–1,3;1,4–1,5	87383.970	−16
4–5	1,3–1,4;1,4–1,5;1,5–1,6	83629.467	−5
1–0	1,1–1,1;1,2–1,1;1,0–1,1	104279.923	−1
2–1	1,1–1,1	109275.362	−6
	1,2–1,1	109276.306	11
	1,3–1,2	109276.841	4
	1,2–1,2	109277.431	−3
	1,1–1,0	109278.224	−21
3–2	1,2–1,2	114221.652	−2
	1,3–1,2;1,4–1,3	114222.790	−38
	1,2,–1,1	114223.216	−10
	1,3–1,3	114223.675	−17
4–3	1,3–1,3	118969.787	−23
	1,4–1,3;1,5–1,4;1,3–1,2	118970.938	−24
	1,4–1,4	118971.804	−3
5–4	1,4–1,4	123508.390	56
	1,6–1,5;1,5–1,4;1,4–1,3	123509.421	−4
	1,5–1,5	123510.275	−26
6–5	1,7–1,6;1,5–1,4;1,6–1,5	127849.480	−4
	1,6–1,6	127850.352	−25
7–6	1,8–1,7;1,6–1,5;1,7–1,6	132009.483	26
$K=1(f)$–0			
1–1	1,1–1,1	101264.966	5
	1,2–1,1	101265.518	1
	1,1–1,2;1,0–1,1	101266.231	19
	1,2–1,2	101266.654	−2
	1,1–1,0	101267.845	6
2–2	1,2–1,2;1,3–1,2;1,1–1,2	102181.501	−12
	1,2–1,3;1,3–1,3	102182.489	−20
	1,2–1,1;1,1–1,1	102183.076	−10
3–3	1,3–1,3	102881.332	−5
	1,4–1,4	102882.140	31
4−4	1,4–1,4	103355.722	19
	1,5–1,5;1,3–1,3	103356.448	4
5–5	1,5–1,5	103620.834	−67
	1,6–1,6;1,4–1,4	103621.550	−18
6–6	1,6–1,6	103702.383	11
	1,7–1,7;1,5–1,5	103703.000	3
7–7	1,7–1,7	103630.489	−19
	1,8–1,8;1,6–1,6	103631.127	17
$K=1(e)$–1(e)			
2–1	1,1–1,1	104320.736	−20
	1,3–1,2;1,2–1,1;1,1–1,0	104321.582	5
	1,2–1,2	104322.164	83
3–2	1,2–1,2	106422.279	−37
	1,2–1,1;1,4–1,3	106423.140	88
	1,3–1,3	106423.878	48
4–3	1,3–1,2;1,5–1,4	108309.306	−14
	1,4–1,3	108309.615	−14
5–4	1,4–1,3;1,6–1,5	110048.792	36
	1,5–1,4	110049.064	19
6–5	1,5–1,4;1,7–1,6;1,6–1,5	111694.466	−7
7–6	1,6–1,5;1,8–1,7;1,7–1,6	113296.241	−18
8–7	1,7–1,6;1,9–1,8;1,8–1,7	114902.614	−1
$K=1(f)$–1(e)			

Table 3 (*continued*)

J'–J''	I', F'–I'', F''	Frequency (MHz)	Observed − calculated (kHz)
1–1	1,1–1,1	96310.340	−9
	1,1–1,2;1,2–1,1	96310.836	10
	1,2–1,2;1,1–1,0	96311.325	18
	1,0–1,1	96311.712	−29
2–2	1,2–1,2;1,3–1,2;1,1–1,2	94382.161	−14
	1,3–1,3	94382.642	−5
3–3	1,3–1,3	92220.111	28
	1,4–1,4;1,2–1,2	92220.517	−16
4–4	1,4–1,4	89895.351	18
	1,5–1,5;1,3–1,3	89895.749	−23
5–5	1,5–1,5	87466.064	28
	1,6–1,6;1,4–1,4	87466.511	25
6–6	1,6–1,6	84989.291	10
	1,7–1,7;1,5–1,5	84989.738	−9

[a] Experimental uncertainties estimated to be 50 kHz.

Table 4
Spectroscopic parameters (in MHz) of the $K=0$ and $K=1$ states of CO–*para*N_2

State		Present	Previous[a]
$(j_{CO}, j_{N_2}) = (0,1)$	B	2143.49(68)	2127.661(42)
$K=0$, $v_{b\_N_2} = 1$	D	0.32127(260)	0.11331(54)
	$H\times10^3$	0.03300(67)[b]	0.03531(14)[b]
	χ_{aa}	−5.1736(100)	−5.1115(18)[c]
	$\chi_{aa\_J}\times10^3$	−4.25(113)	
	$C\times10^3$	9.68(111)	11.49(74)/−33.0(24)[d]
$K=1$	σ	4573.69(68)	4586.637(41)
$K=1(e)$	B	2105.35(67)	2123.447(41)
	D	0.08521(256)	0.30071(55)
	$H\times10^3$	0.03300(67)[b]	0.03531(14)[b]
	χ_{aa}	0.5661(120)	0.5235(18)
	χ_{bb}	0.0488(107)	−0.0134(20)
	$C\times10^3$	−7.31(1.9)	−18.7(25)/−4.74(80)[d]
$K=1(f)$	B	2249.41814(76)	2249.41897(17)
	D	0.133447(63)	0.133477(13)
	$H\times10^3$	−0.11290(143)	−0.11293(29)
	χ_{aa}	0.5702(127)	0.5353(18)
	χ_{bb}	−3.0369(121)	−3.0017(3)
	$\chi_{bb\_j}\times10^3$	4.46(131)	
	$C\times10^3$		11.49(74)/−33.0(24)[d]
Interaction constants of $K=1(e)$ and	G	2176.26(77)	2158.224(48)
$K=0$	G_J	−3.3932(122)	−3.01458(74)
	$G_{JJ}\times10^3$	1.799(78)	
$(j_{CO}, j_{N_2}) = (1,1)$	σ	102278.4553(188)	
$K=1$	B	1996.7822(75)	
	D	−0.26810(82)	
	$H\times10^3$	−1.590(35)	
	$L\times10^6$	7.38(62)	
	$M\times10^6$	−0.0193(40)	
	b	−4.5304(62)	
	d	0.05556(64)	
	$h\times10^3$	−0.2378(206)	
	$l\times10^6$	1.306(198)	
	χ_{aa}	−1.850(43)	
	χ_{bb}	−0.005(36)	

[a] Values from the work of Xu and Jäger [16].
[b] The values of H for both $K=0$ and $K=1$ stacks were constrained to the same value in the fit.
[c] A value of 8.440(68) was obtained for χ_{bb} in the work of Xu and Jäger [16].
[d] Two spin-rotation constants C_{aa} and C_{bb} were used in fit in work of Xu and Jäger [16].

$(j_{CO}, j_{N_2}) = (1,1)$ state should include three stacks with $K=0$, two pairs of stacks with $K=1$, and one pair of stacks with $K=2$. The existence of interactions between some of them and the newly observed $K=1$ states is supported by the negative values of b and D of the observed $K=1$ stack.

We could not determine any transitions connecting the unperturbed lower $K=1(f)$ levels with the newly detected levels by our assignment process in spite of additional deep searches based on the known location of the lower $K=1(f)$ stack of (0,1) manifold from the MW and IR works [16,17].

5. Discussion

In the case of the CO–*ortho*N_2 spin modification, the new information presented here concerns at first the observation of the Q-branch of the $K=1$–0 subband. Together with our previous observation of the R-branch transitions [15] it gives precise determination of σ, the $K=1$ stack origin, and its asymmetry splitting. Both parameters can be used to characterize the degree of strength of van der Waals bond or degree of rigidity of the complex. In the free rotor limit, the $K=1$ splitting achieves a value of $2B$ for the complex, i.e. it would be 0.148 cm^{-1} in the case of CO–*ortho*N_2. The measured value of only 0.008 cm^{-1} just reveals the asymmetry of the complex and indicates its seemingly quite rigid behavior. On the other side, in a rigid T-shaped rare gas CO complex, the separation of the ground $K=0$ and 1 stacks would be 1.92 cm^{-1} (the value of the rotational constant of the CO monomer, b_{CO}). In the case of free rotation of the CO unit, the separation would be $2b_{CO}$, or 3.84 cm^{-1}. The corresponding energy difference for CO–*ortho*N_2 is 3.534 cm^{-1}, very close to the free rotation limit, and it falls between Ne–CO and He–CO cases. The bending state of CO–*ortho*N_2, which was found earlier to lie 4.667 cm^{-1} above the ground state [17,18], is lower than for all Rg–CO and CO–H_2 systems. This also suggests that the CO rotation is relatively free. The contradiction between locations of different K-stacks and the amount of $K=1$ splitting illustrates that CO–N_2 is not close to any limiting case of free or semirigid rotor.

The MW study of Xu et al. [15] revealed that the ground state of CO–*ortho*N_2 has an approximate T-shaped structure with N_2 forming the top and CO forming the leg, and that the oxygen atom is closer to the N_2 subunit than the carbon atom. The same study suggested that the lower $K=1$ state of CO–*ortho*N_2 has a different geometry with N_2 forming the leg and CO forming the top. Comparing the coupling constants χ_{aa} and rotational constants B for lower and upper $K=1$ states (see Tables 5 and 6), we can propose a similar geometry for the upper $K=1$ state but with slightly shorter distance between the monomers.

In the $K=0$ state of CO–*para*N_2, the N_2 subunit is remarkably localized in the parallel direction with respect to the intermolecular axis, while in the low $K=1$ state complex has an O bonded structural orientation with the N_2 subunit on average in a more perpendicular orientation with respect to the intermolecular axis [16]. The new information of the present work concerns the detection of an upper $K=1$ stack and its identification as belonging to the $(j_{CO}, j_{N_2}) = (1,1)$ free rotor state. This state is located at 3.41 cm^{-1} above the ground $K=0$ state of CO–*para*N_2 and represents nearly free simultaneous rotation of both monomers. As mentioned above, we actually expect a total of nine stacks of levels arising from $(j_{CO}, j_{N_2}) = (1,1)$: three $K=0$, two pairs with $K=1$, and one stack with $K=2$. Therefore, the identity of the new $K=1$ state is still somewhat ambiguous. In the infrared study [17] one of two $K=1$ stacks and one $K=2$ stack belonging to manifold $(j_{CO}, j_{N_2}) = (1,1)$ were observed in the vibrational excited state

Table 5
Comparison of CO–N_2 rotational constants (in MHz)

Modification	(j_{CO}, j_{N_2})	$K=0$	$K=1(e)$	$K=1(f)$
ortho	(0,0)	2227.54[a]		
ortho	(1,0)	2089.75[b]	2078.88[a]	2205.08[a]
para	(0,1)	2143.49[a]	2105.35[a]	2249.42[a]
para	(1,1)		1999.05[a]	1994.52[a]

The $K=1(e)$ and $K=1(f)$ states were fitted with separate B values.
[a] Present work.
[b] Surin et al. [18].

Table 6
Comparison of CO–N_2 nuclear quadrupole coupling constants (in MHz)

Modification	(j_{CO}, j_{N_2})	χ_{aa}			χ_{bb}	
		$K=0$	$K=1(e)$	$K=1(f)$	$K=1(e)$	$K=1(f)$
ortho	(0,0)	0.205[a]				
ortho	(1,0)	−0.768[b]	−1.039[a]		0.061[a]	0.166[a]
para	(0,1)	−5.174[a,c]	0.566[a]	0.570[a]	0.049[a]	−3.037[a]
para	(1,1)		−1.850[a]		−0.005[a]	

[a] Present work.
[b] Surin et al. [18].
[c] A value of 8.44 MHz was obtained for χ_{bb} by Xu and Jäger [16].

Table 7
Calculated energy levels (cm^{-1}) of CO–*ortho*N_2

J	$(j_{CO}, j_{N_2}) = (0,0)$	$(j_{CO}, j_{N_2}) = (1,0)$		
	$K=0$	$K=1(e)$	$K=1(f)$	$K=0$
0	0.000000	–	–	4.666311
1	0.148588	3.600899	3.609322	4.805719
2	0.445656	3.878096	3.903390	5.084510
3	0.890991	4.293447	4.344107	5.502630
4	1.484264	4.846423	4.931005	6.060003
5	2.225031	5.536327	5.663453	6.756522
6	3.112718	6.362305	6.540649	7.59206
7	4.146593	7.323364	7.561592	8.56645
8	5.32571	8.418377	8.72504	9.67952
9	6.64878	9.64608	10.02939	10.9311
10	8.1140	11.00502	11.4725	12.3208
11	9.7184	12.4934	13.0512	
12	11.458	14.1087	14.761	
13	13.324	15.847	16.594	
14	15.305	17.703	18.538	
15	17.379	19.664	20.572	
16	19.51	21.715	22.66	
17	21.65	23.82	24.76	
18	23.71	25.94	26.78	
19	25.55	27.99	28.60	

The uncertainty of each level is in the last quoted digit.

Table 8
Calculated energy levels (cm^{-1}) of CO–*para*N_2

J	$(j_{CO}, j_{N_2}) = (0,1)$			$(j_{CO}, j_{N_2}) = (1,1)$	
	$K=0$	$K=1(e)$	$K=1(f)$	$K=1(e)$	$K=1(f)$
0	0.000000	–	–	–	–
1	0.100226	0.265515	0.22759	3.478404	3.478109
2	0.336031	0.596203	0.52761	3.745307	3.744466
3	0.712766	1.068397	0.97738	4.146097	4.144538
4	1.231281	1.680277	1.57655	4.681210	4.678873
5	1.891631	2.430504	2.32467	5.351112	5.348067
6	2.693548	3.317753	3.22115	6.156231	6.152701
7	3.636539	4.340622	4.26526	7.096909	7.093294
8	4.719911	5.497616	5.45608	8.173360	8.170297

The uncertainty of each level is in the last quoted digit.

of the CO stretch, $\nu_{CO}=1$. The $K=1$ stack was attributed to the state involving rotation of the CO unit in the plane perpendicular to the intermolecular axis and rotation of N_2 unit in the plane containing the intermolecular axis (bending vibration). Interestingly, we observed the same subbands involving the new $K=1$ state of the region $(j_{CO}, j_{N_2}) = (1,1) - (0,1)$ for the ground state $\nu_{CO}=0$ as in the infrared work: *P*- and *R*-branches of $K=1(e)-0$, *Q*-branch of $K=1(f)-0$, *R*-branch of $K=1(e)-1(e)$ and one additional *Q*-branch of $K=1(f)-1(e)$ subband. No transitions connecting a $K=1$ state with the lower $K=1(f)$ were detected. One more common point of the new $K=1$ states in both studies is, that their *B* constants are very similar, and they are the smallest relative to all other known states of the CO–N_2 complex (see Table 5). Finally, the negative value of the χ_{aa} quadrupole constant of the new $K=1$ state (see Table 6) also suggests that the N_2 subunit is more localized in the parallel direction with respect to the intermolecular axis. It allows us to identify the new $K=1$ state as the state involving rotation of the CO unit in the plane perpendicular to the intermolecular axis and rotation of the N_2 unit in the plane containing the intermolecular axis.

The present study confirms the previous IR [12,13,17] and MW [14–16,18] investigations, that the CO–N_2 complex is a rather complicated molecule, which is not expected to be close to any limiting case of free or semirigid rotor or to have simple energy level patterns. Many unassigned millimeter wave transitions of different intensity and different hyperfine structure have been observed. We suppose, that these transitions connect the still unknown states of the *para*N_2 modification, namely of the $(j_{CO}, j_{N_2}) = (1,1)$ manifold, and states of the already well studied $(j_{CO}, j_{N_2}) = (0,1)$ manifold. The detection and assignment of these not yet identified stacks will be a subject of future millimeter wave surveys.

As already mentioned, the theoretical work on the CO–N_2 intermolecular potential is limited by only the semiempirical result reported by Francken and Dykstra [9] and an ab initio study by Fišer et al. [10,11]. In spite of the fact, that similar geometries and intermolecular separations as compared to experiment were established by the ab initio study [10,11], the ordering of calculated interaction energies for these geometries is reversed with respect to experiment. More extensive calculations are necessary in order to describe the already numerous experimental data. For direct comparison with possible future theoretical studies we predicted the energies of rotational levels of the CO–*ortho*N_2 and –*para*N_2 modifications from our fit model. The energies are given in Tables 7 and 8, respectively.

In summary, this work presents the millimeter wave observation of *Q*- and *P*-branches of the $K=1$–0 subband of the CO–*ortho*N_2 spin modification. For the less abundant form, CO–*para*N_2, a new state with $K=1$ located at 3.41 cm^{-1} relative to the lowest $K=0$ state of CO–*para*N_2 was observed for the first time. This state represents simultaneous nearly free rotation of both monomers inside the complex.

Acknowledgements

The work was supported by the Forschungsgruppe Laborastronomie (FGLA). HSPM thanks DFG for a support through Research Grant SFB-494. The work of AVP, VAP and BSD at Cologne was made possible by the DFG through a grant aimed to support Eastern and Central European Countries and Republics of the FSU (436RUS113/719/0-2) and through the Leonhard–Euler Fellowship Program by the DAAD (A04/00926). The support of the Russian Foundation for Basic Research (RFBR: 03-02-17478-a and 05-02-04008-a) is gratefully acknowledged by BSD, AVP and VAP.

References

[1] See, for example L.H. Coudert, I. Pak, L. Surin, J. Chem. Phys. 121 (2004) 4691 (and references therein).
[2] See, for example L.A. Surin, A.V. Potapov, V.A. Panfilov, B.S. Dumesh, G. Winnewisse, J. Mol. Spectrosc. 230 (2005) 149 (and references therein).
[3] A.R.W. McKellar, Y. Xu, W. Jäger, C. Bissonnette, J. Chem. Phys. 110 (1999) 10766.
[4] L.A. Surin, D.A. Roth, I. Pak, B.S. Dumesh, F. Lewen, G. Winnewisser, J. Chem. Phys. 112 (2000) 4064; Erratum, J. Chem. Phys. 112 (2000) 9190.
[5] A.R.W. McKellar, J. Chem. Phys. 108 (1998) 1811.
[6] I. Pak, L.A. Surin, B.S. Dumesh, D.A. Roth, F. Lewen, G. Winnewisser, Chem. Phys. Lett. 304 (1999) 145.
[7] A.R.W. McKellar, J. Chem. Phys. 112 (2000) 9282.
[8] L.A. Surin, B.S. Dumesh, G. Winnewisser, I. Pak, J. Chem. Phys. 113 (2000) 9351.

[9] K.A. Franken, C.E. Dykstra, J. Phys. Chem. 97 (1993) 11408.
[10] J. Fišer, R. Polák, Chem. Phys. Lett. 360 (2002) 565.
[11] J. Fišer, T. Boublík, R. Polák, Mol. Phys. 101 (2003) 3409.
[12] Y. Kawashima, K. Nishizawa, Chem. Phys. Lett. 249 (1996) 87.
[13] Y. Xu, A.R.W. McKellar, J. Chem. Phys. 104 (1996) 2488.
[14] Y. Kawashima, Y. Ohshima, Y. Endo, Chem. Phys. Lett. 315 (1999) 201.
[15] Y. Xu, W. Jäger, L.A. Surin, I. Pak, V.A. Panfilov, G. Winnewisser, J. Chem. Phys. 111 (1999) 10476.
[16] Y. Xu, W. Jäger, J. Chem. Phys. 113 (2000) 514.
[17] C. Xia, A.R.W. McKellar, Y. Xu, J. Chem. Phys. 113 (2000) 525.
[18] L.A. Surin, H.S.P. Müller, E.V. Alieva, B.S. Dumesh, G. Winnewisser, I. Pak, J. Mol. Struct. 612 (2002) 207.
[19] L.A. Surin, B.S. Dumesh, F. Lewen, D.A. Roth, V.P. Kostromin, F.S. Rusin, G. Winnewisser, I. Pak, Rev. Sci. Instrum. 72 (2001) 2535.
[20] J. Tang, A.R.W. McKellar, L.A. Surin, D.N. Fourzikov, B.S. Dumesh, G. Winnewisser, J. Mol. Spectrosc. 214 (2002) 87.
[21] L.A. Surin, D.N. Fourzikov, F. Lewen, B.S. Dumesh, G. Winnewisser, A.R.W. McKellar, J. Mol. Spectrosc. 222 (2003) 93.
[22] H.M. Pickett, J. Mol. Spectrosc. 148 (1991) 371.